Ionizational and Electron Thermal Nonequilibrium in MHD Boundary Layers

DONALD W. COTT*
North Carolina State University, Raleigh, N.C.

The effects of thermal nonequilibrium (elevated electron temperatures), and ionizational nonequilibrium (finite-rate recombination) are studied in the insulator boundary layer of a potassium-seeded nitrogen MHD accelerator. The nonsimilar, compressible boundary layer is assumed steady, laminar, and two-dimensional. A collisionless sheath is assumed and matched with the continuum boundary-layer equations through a transition region, the physics of which is dominated by ambipolar diffusion. Numerical results are presented for a typical core flow Hall-neutralized Faraday accelerator. Profiles are presented demonstrating the gradual development of severe B-wall shorting with the best available values of energy-loss factor and recombination rate coefficient. The relative importance of the various terms in the electron energy equation is assessed, and the need for more accurate energy exchange cross sections is pointed out by the high sensitivity of the solutions to energy-loss factor. An unexpected result is that finite-rate recombination is not particularly important for the class of accelerators under study, although it could well be important for other applications, such as noble gas generators.

Nomenclature

B = magnetic field intensity in z direction
SF = mass fraction of potassium seed nuclei
C_p = specific heat at constant pressure
C_s = mass concentration of species s, ρ_s/ρ
E_x,E_y = electric field strength in x and y directions, respectively
e = absolute charge on an electron
H = stagnation enthalpy, $h + u^2/2$
h = static enthalpy
J_x,J_y = total current density due to electrons, sum of conducted and convected electron current densities, i.e., $J_x = j_x - n_e e u$
j_x,j_y = electron conducted current density, see Eqs. (6) and (7)
k = Boltzmann's constant
k_e = electron thermal conductivity, see Eq. (20)
l = channel semiwidth in z direction
m_{rs} = reduced mass
m_s = rest mass of a single particle of species s
n_s = number density of particles of species s
Pr = Prandtl number
p = pressure
Q_{sr} = collision cross section for momentum exchange between species s and species r
q_s = heat flux due to species s
R = over-all gas constant
T = temperature
u,w = mass average velocity in x and z directions
x,y,z = channel flow coordinate system, see Fig. 1
Z = compressibility factor, see Eq. (12)
α_{rec} = recombination rate coefficient
β = Hall parameter, $\sigma_e B/n_e e$
Γ_s = diffusion flux of species s in z direction
δ = boundary-layer thickness at $u/u_\infty = 0.95$
δ_s = energy-loss factor, a multiplying factor included in the energy collision integral to account for inelastic collisions; for perfectly elastic collisions $\delta_s = 1$
ϵ_{rec} = recombination energy for ions
λ_d = Debye length
λ_e = electron mean free path
μ = over-all gas viscosity
ν_o = over-all electron collision frequency, see Ref. 12
ν_{sr} = effective collision frequency between particles of s and r species, $\nu_{sr} = \dfrac{4\pi n_r m_{rs}}{3n_s kT_s}\displaystyle\int_0^\infty Q_{sr}c^5 f_s dc$
ρ = mass density
$\partial\rho_e/\partial t$ = rate of production of electrons through chemical reaction
σ_o,σ_e = electrical conductivity, first and second order approximations, respectively, see Ref. 12
σ_i = ion electrical conductivity, $n_i e^2 \Big/ \sum_s m_{is}\nu_{is}$

Superscript

$*$ = Saha equilibrium condition

Subscripts

e = electron species
o = values at outer edge of sheath
r,s = species r or species s, respectively
∞ = core flow condition

Presented as Paper 71-138 at the AIAA 8th Aerospace Sciences Meeting, New York, January 25-27, 1971; submitted October 21, 1970; revision received July 6, 1971. This work was sponsored by Headquarters, AEDC, Arnold Air Force Station, Tenn., through Contract F40600-69-C-0001. The author wishes to thank L. E. Ring, M. D. High, G. W. Garrison, and Paul Johnson for their many helpful suggestions throughout the course of this work.

Index categories: Plasma Dynamics and MHD; Electric Power Generation Research; Boundary Layers and Convective Heat Transfer-Laminar.

* Assistant Professor of Mechanical and Aerospace Engineering. Associate Member AIAA.

Introduction

In recent years a great deal of interest has been focused on the effects of elevated electron temperature and nonequilibrium recombination on the performance of magnetohydrodynamic (MHD) accelerators and generators. The problem is particularly acute for accelerators, where higher current densities tend to elevate the electron temperature, which in turn drastically affects the electrical conductivity. Hale and Kerrebrock[1] have examined the effects of elevated electron temperatures on the insulating B-walls of noble gas MHD generators. They assumed, however, that the electron concentration was in local equilibrium, as evaluated by Saha's equation at the electron temperature. For practical accelerators and generators, this Saha equilibrium assumption is adequate in the core flow and across most of the boundary layer. Near the wall, however, there is evidence which suggests that the electron concentration is governed by finite recombination rates. In this case, the very strong coupling between electron temperature and electrical conductivity, through Saha's equation, is considerably modified. If this ionizational nonequilibrium assumption extends very far out into the boundary layer then the effect on the over-all boundary layer might be significantly different than earlier analyses indicate.

Quite recently Sherman, Yeh, Reshotko, and McAssey[2] have presented a paper dealing with the electrode insulator wall in the plane of the electric field. Their treatment of the electron energy equation is comparable in degree of sophistication to the present work. Their treatment of the electron concentration equation, however, neglects the diffusion term, which for some applications could be quite important. Neglecting the diffusion term obviates a wall boundary condition on electron concentration, thus the free molecular sheath analysis is simplified and no transition region is introduced.

The purpose of this study is to provide insight into the relative importance of elevated electron temperature and nonequilibrium recombination in typical accelerators. The flow in a Faraday accelerator is studied, using potassium seeded nitrogen as a working fluid. Only the insulator, or B-wall, is considered, since this is where the most potentially detrimental effects are expected to occur. To make the problem more tractable, steady, two-dimensional, laminar flow is assumed in the plane of the magnetic field. A nonsimilar, implicit, numerical technique is used to calculate the flow field in the continuum region, and this is carefully coupled to a relatively simple collisionless sheath model.

In defense of the laminar flow assumption, it is emphasized that the primary motivation for undertaking this work was to shed light on the relative influence of various nonequilibrium phenomena in laminar boundary layers, since this relative influence is likely to be similar in turbulent boundary layers. Simplifications which are applicable to subsequent turbulent calculations are suggested in the section entitled "Conclusions." Also the two-dimensional flow assumption neglects the three-dimensional swirl imparted to the flow by the Hall current Lorentz force. This assumption is motivated primarily by computational considerations, although the results of Hale and Kerrebrock[1] indicate that at moderate Hall parameters the swirl effect is small.

Physical Model

The equations of motion, auxiliary relations, and sheath equations are derived by Cott[3] from basic considerations, in a development patterned in part after those of Sutton and Sherman,[4] and Sherman et al.[2]

Equations of Motion

In boundary-layer form the equations of motion are as follows:

Over-all continuity

$$\partial(\rho u)/\partial x + \partial(\rho w)/\partial z = 0 \tag{1}$$

Over-all momentum

$$\rho u \frac{\partial u}{\partial x} + \rho w \frac{\partial u}{\partial z} = -\frac{dp}{dx} + j_y B + \frac{\partial}{\partial z}\left(\mu \frac{\partial u}{\partial z}\right) \tag{2}$$

Over-all energy

$$\rho u \frac{\partial H}{\partial x} + \rho w \frac{\partial H}{\partial z} = \frac{\partial}{\partial z}\left(\frac{\mu}{Pr}\frac{\partial H}{\partial z}\right) + \frac{\partial}{\partial z}\left[\left(1 - \frac{1}{Pr}\right)\frac{\mu}{2}\frac{\partial(u^2)}{\partial z}\right] + j_x E_x + j_y E_y - \frac{\partial}{\partial z}\left\{\left[\frac{5k}{2}(T + T_e) + \epsilon_{\text{rec}}\right]\Gamma_e\right\} + \frac{\partial}{\partial z}\left[k_e \frac{\partial T_e}{\partial z}\right] \tag{3}$$

The practical description of the electron gas within the framework of the over-all multispecies plasma is an inherently controversial subject. This is particularly so when the application involves boundary layers, for which it is notoriously difficult to estimate the importance of a given term a priori. Since the objective of this effort is to investigate the electron nonequilibrium effects in the boundary layer, the gradient terms normal to the wall are retained in the electron concentration, momentum, and energy equations. Convection terms are retained in Eqs. (4) and (5), although they are neglected in the electron momentum equation, which in component form is Eqs. (6–8). The dominant mechanisms of energy exchange between electrons and other species are assumed to be inelastic collisions with nitrogen molecules, and three-body recombination with the potassium seed ions. Actually elastic collisions with potassium neutrals and coulomb collisions with potassium ions were included in the calculations, but they turned out to be negligible and so are eliminated here for brevity. Energy transfer from the electron gas due to electronic excitation of the potassium neutrals is neglected, restricting the analysis to relatively low electron temperatures (below 8000°R). This may seem inconsistent since recombination and ionization are accounted for in Eq. (4). But while ionization and recombination are critical as regards the electron concentration, the resultant energy transfer is small, as calculated in the recombination term of Eq. (5). This lends some credence to the assumption that the energy transfer due to electronic excitation of potassium is negligible at temperatures below 8000°R.

Vibrational equilibrium is assumed for simplicity, and can be justified a posteriori, in the region where severe B-wall shorting does not exist. There is little doubt that severe B-wall shorting involves some degree of vibrational nonequilibrium, and that it tends to have a damping influence on the electron temperature overshoot. Thus the vibrational energy rate equation should be included if high quantitative accuracy is desired in a region dominated by B-wall shorting. Such a three-temperature model must also include heavy species interactions, such as nitrogen-vibrational to potassium-electronic resonance phenomena.

For the two-temperature electron description adopted here, the equations are derived from Boltzmann's Equation in the thesis version of Ref. 3, and are presented as follows:

Electron concentration

$$\rho u \frac{\partial C_e}{\partial x} + \rho w \frac{\partial C_e}{\partial z} = -\frac{\partial}{\partial z}[m_e \Gamma_e] + \frac{\partial \rho_e}{\partial t} \tag{4}$$

Electron energy

$$\rho u \frac{\partial T_e}{\partial x} + \rho w \frac{\partial T_e}{\partial z} = \frac{1}{C_e}\frac{\partial}{\partial z}\left(\frac{k_e}{C_{p,e}}\frac{\partial T_e}{\partial z}\right) - \frac{m_e \Gamma_e}{C_e}\frac{\partial T_e}{\partial z} + \frac{e\rho u j_x}{m_e C_{p,e} \sigma_o} + \frac{E_x J_x + E_y J_y}{C_e C_{p,e}} - \frac{6}{5}\rho \frac{m_e}{m_{N_2}} \delta_{N_2} \nu_{eN_2}(T_e - T) - \frac{1}{C_e}\left(T_e + \frac{2\epsilon_{\text{rec}}}{5k}\right)\frac{\partial \rho_e}{\partial t} \tag{5}$$

where the notation is defined in the Nomenclature, and the

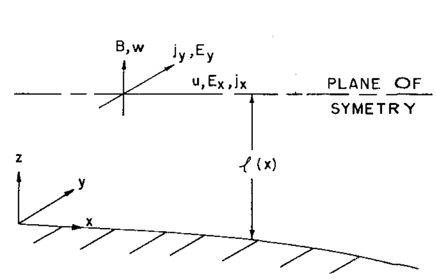

Fig. 1 Channel flow coordinate system.

coordinate system is illustrated in Fig. 1. The auxiliary relations are as follows:

Ohm's Law

$$j_y = \frac{\sigma_e(E_y - uB) + \beta^2 j_{y,\infty}(n_e/n_{e,\infty})}{1 + \beta^2} \tag{6}$$

$$j_x = \beta j_y[(j_{y,\infty}/j_y)(n_e/n_{e,\infty}) - 1] \tag{7}$$

Ambipolar diffusion

$$\Gamma_e = -(m_e/\rho e^2 C_e)[\sigma_e\sigma_i/(\sigma_e + \sigma_i)]\partial/\partial z(p_e + p_i) \tag{8}$$

Recombination

$$\frac{\partial\rho_e}{\partial t} = \alpha_{\text{rec}}\frac{\rho^3 C_e}{(m_e)^2}\left[\left(\frac{C_e^2}{C_K}\right)^*\left(SF - \frac{m_K}{m_e}C_e\right) - C_e^2\right] \tag{9}$$

State

$$p = \rho ZRT \quad \text{and} \quad p_s = (k/m_s)\rho C_s T_s \tag{10}$$

Saha equilibrium

$$C_e^* = [2m_e/(\psi_1 m_{N_2})]\{[1 + \psi_1(m_{N_2}/m_K)SF]^{1/2} - 1\} \tag{11}$$

where

$$\psi_1 = 4p/(K_s kT)$$

$$K_s = \frac{n_i n_e}{n_K} = 2.41 \times 10^{21}\, T_e^{3/2}\, Z_{rs}\exp(-50{,}408/T_e)$$

and

$$Z_{rs} = 9.11 \times 10^{-1} + 7.33 \times 10^{-5}T - 1.49 \times 10^{-8}T^2$$

where T and T_e are in degrees Kelvin.

Gas Properties

For the nitrogen background gas, R and Pr are assumed constant at 1776 ft^2/sec^2-°R and 0.75, respectively. The following expressions are used for the remaining over-all gas properties:

$$Z = 1 + 276.6\left[\frac{3.661 \times 10^{-3}T}{p}\right]^{.4964}\exp(-55{,}831/T) \tag{12}$$

$$\frac{C_p}{R} = 3.5 + 1.514 \times 10^{-5}T + \left[\frac{\theta_v/T}{\exp(\theta_v/T) - 1}\right]^2 \times \exp(\theta_v/T) + (Z - 1)\left[1 + (T + 1.125 \times 10^5) \times \left(\frac{0.4964}{T} + \frac{55{,}831}{T^2}\right)\right] \tag{13}$$

$$\mu = [1.21 \times 10^{-5}\text{lbm/(ft-sec)}][T/300°\text{K}]^{0.668} \tag{14}$$

where T is in °K and p is in atmospheres. Eqs. (12) and (13) are due to Ring[5] and are valid within a temperature range from 200 to 5000°K. Equation (14) is a curve fit to calculations by Baulknight[6] and is accurate to within 3% from 300 to 5000°K.

The three-body recombination reaction

$$K + e^- \rightleftarrows K^+ + 2e^- \tag{15}$$

is considered to be the dominant reaction in this analysis. The kinetics of this reaction have been studied by Curry,[7] Cool and Zukoski,[8] and Dugan,[9] for potassium and other alkali metals. Calculations from these references have been distilled by Demetriades[10] into the curve fit

$$\alpha_{\text{rec}} = 3.47 \times 10^{-20}T_e^{-4.765} \tag{16}$$

where the recombination rate coefficient, α_{rec}, is in m^6/sec, and T_e is in °K. The ion electrical conductivity, σ_i, is calculated using the following curve fit:

$$Q_{iN_2} \approx 2.39 \times 10^{-17}T^{(1.756\times10^{-5}T - 0.5)} \tag{17}$$

from integrated potassium ion-nitrogen cross sections in Weber and Templemeyer.[11] The over-all electrical conductivity, σ_e, is calculated using the methods of Demetriades and Argyopolous,[12] which take into account both thermal and ionizational nonequilibrium. These calculations are based on collision cross sections from Garrison,[13] as follows:

$$Q_{eK} = 4.0 \times 10^{-18} \tag{18}$$

$$Q_{eN_2} = 4.5565 \times 10^{-20} + 2.81786 \times 10^{-23}T_e - 4.99704 \times 10^{-27}T_e^2 + 3.30643 \times 10^{-31}T_e^3 \tag{19}$$

where Q_{eK} and Q_{eN_2} are in meters^2, and T_e is in °K.

Evaluation of the electron thermal conductivity, k_e, is also based on Ref. 12, resulting in

$$k_e = \left[\frac{ek}{m_e}\frac{n_e}{\nu_0}\right]^2 T_e\left[\frac{1}{\sigma_0} - \frac{1}{\sigma_e}\right] \tag{20}$$

where ν_0 and σ_0 are defined in Ref. 12.

The species energy-loss factor δ_{N_2} is based on experiments by Demetriades,[14] and for diatomic nitrogen assumes the value of 18. Note that this is based on an elastic energy-loss factor of 1.

Boundary Conditions

The sheath analysis is broken up into three regions. The first region is that nearest the wall, the electrostatic sheath itself, where electrostatic forces dominate the diffusion of electrons and ions to the wall. Here it is assumed that collision effects are negligible. This assumption is marginal but it turns out that the over-all solutions are not strongly sensitive to it.[3] The second region is the transition region, which acts as the buffer region between the collisionless sheath and the collision dominated boundary-layer flow. In this transition region, momentum and energy transfer due to collisions is accounted for, but recombination is neglected. This region is somewhat arbitrarily extended from about one Debye length to approximately one thousand electron mean-free-paths from the wall. The character of the flow is dominated by ambipolar diffusion in this region, with the influence of collisional energy transfer being felt near the outer edge, where the transition region merges into the collision dominated, continuum flow region. The flow in the third region, the continuum boundary-layer region, is described by the continuum boundary-layer equations, including the effects of ambipolar diffusion, finite recombination rates, and electron thermal nonequilibrium. This region extends from about one thousand mean-free-paths from the wall, to the channel center plane.

The electrostatic sheath equations are derived in Ref. 3, in the following form:

$$\Gamma_{e,0} = -\frac{\rho_0 C_{e,0}}{m_e}\left[\frac{kT_0}{2\pi m_i}\right]^{1/2} \tag{21}$$

$$q_{e,0} = -\frac{\rho_0 C_{e,0} kT_{e,0}}{2m_e}\left[\frac{kT_0}{2\pi m_i}\right]^{1/2}\left[4 + \ln\left(\frac{T_{e,0}m_i}{T_0 m_e}\right)\right] \tag{22}$$

which yield the electron flux $\Gamma_{e,0}$, and the $q_{e,0}$, at the edge of the sheath (denoted by 0 subscript) in terms of C_e and T_e at that point. Thus if $C_{e,0}$ and $T_{e,0}$ are known, then $\Gamma_{e,0}$ and $q_{e,0}$ can be used as boundary conditions on the wall side of the transition region.

The transition region is described by assuming that the flux terms and the collisional energy term dominate in Eqs. (4) and (5), yielding

$$(d/dz)(\Gamma_e) = 0 \tag{23}$$

and

$$\frac{dq_e}{dz} = -3kn_e \frac{m_e}{m_{N_2}} \delta_{N_2}\nu_{eN_2}(T_e - T) \quad (24)$$

Note that these transition equations are not dependent on continuum assumptions, and thus are compatible on one side with the free molecular sheath and on the other side with the continuum boundary layer region. For the present purposes it is sufficiently accurate to consider the right side of Eq. (24) constant across the transition region, as evaluated at the outer edge of the sheath. With this simplification it is simple to solve the first order, total differential equations for Γ_e and q_e, with the boundary conditions at $z \approx \lambda_d$ as given by Eqs. (21) and (22), the sheath equations. The result is known values for Γ_e and q_e at the transition-continuum interface. Since continuum effects predominate at this interface, Eq. (8) is valid for Γ_e, and q_e can be expressed by the usual continuum expression

$$q_e = -k_e \frac{dT_e}{dz} + m_e h_e \Gamma_e \quad (25)$$

Note that for the conditions of this problem the transition-continuum interface ($z \approx 1000\ \lambda_e$) is less than one tenth of the way across the boundary layer; thus the flow is essentially Couette flow, and partial derivatives in the z-direction can be approximated as total derivatives. It also is possible to neglect the z-variation of T_e and ρ in the pressure derivative of Eq. (8), in comparison to the much larger variation of C_e.

With the foregoing approximations, Eq. (8) can be solved for dC_e/dz at the transition-continuum interface. This serves as the wall boundary condition for Eq. (4), the continuum electron diffusion equation. Similarly Eq. (25) can be solved for dT_e/dz, which serves as the wall boundary condition for Eq. (5), the continuum electron energy equation. This method thus serves as a physically reasonable and self-consistent (albeit approximate) way of relating the free molecular sheath to a continuum boundary layer.

The continuum boundary-layer equations are solved in their full complexity to the channel center plane. The center plane boundary conditions are then found by dropping all transverse terms. Thus, the solutions are only valid for a channel entrance flow to the point where the boundary-layers merge.

Numerical Procedure

Equations (1–5), the continuum boundary-layer equations are solved using a nonsimilar, implicit, finite-difference technique developed originally for turbulent flow by Patankar and Spalding.[15,16] The modifications necessary for this application are presented in Ref. 3. This technique was chosen for several reasons, chief of which was the fact that it would facilitate the later extension of the solution into the turbulent flow regime.

Results

Computer calculations are discussed in detail in this section for the actual physical case, which involves the simultaneous presence of electron thermal nonequilibrium and ionizational nonequilibrium. The effects of varying the energy-loss factor δ_{N_2} are presented, with a physically realistic recombination rate coefficient α_{rec}. Then with a physically realistic δ_{N_2}, the effects of varying α_{rec} are explored.

Simultaneous Thermal and Ionizational Nonequilibrium

In order to obtain a physically meaningful standard of comparison, the first channel flow solution was run with $\delta_{N_2} = 18$ and α_{rec} as given in Eq. (16), which were felt to be the most realistic values currently available. The results of this computation are presented in Figs. 2 and 3. All of the calculations reported herein were run with potassium seeded (1% by mole) nitrogen.

Figure 2a shows the geometry of the accelerator section, and the configuration of the electric and magnetic fields. The nature of the core flow was primarily determined by fixing the magnetic field B, the transverse current density $j_{y,\infty}$, and the static temperature T_∞, constant in the core flow throughout most of the channel; with values of 2 web/m², 15 amps/cm² and 6300°R. The pressure variation and the area variation where then determined using techniques described in Ref. 3, rather than being prescribed a priori. It should be pointed out here that it is useful to use this method of specified temperature variation to design a channel, and then proceed with a prescribed area variation to examine the channel performance for off design conditions, see Ref. 3 for the details of this procedure. At the entrance of the channel there were no fields present, with B being increased linearly from zero at $x/l_0 = 0$ to its full value at $x/l_0 = 10$. E_y was calculated from Ohm's Law, assuming a linear buildup of $j_{y,\infty}$ to its full value at $x/l_0 = 10$. Throughout the channel, E_x was varied according to Eq. (7), to keep the core flow Hall-neutralized ($j_{x,\infty} = 0$). The variations of core flow pressure, temperature, and velocity down the channel are plotted in Fig. 2b. It should be emphasized at this point that Maxwell's equations are not rigorously satisfied in the entry region. Therefore the solutions presented in this investigation are not necessarily valid where $0 \leq x/l_0 \leq 10$.

Figure 3 illustrates the development of the boundary-layer profiles as they proceed down the channel. The most important effect which is illustrated is the presence of B-wall shorting in about the last third of the channel. This is most evident in the current density profiles. Figures 3c and 3d, which add vectorially to a maximum current density of 122 amps/cm², at $z/\delta = 0.34$ and $x/l_0 = 120$. T_e and C_e, Figs.

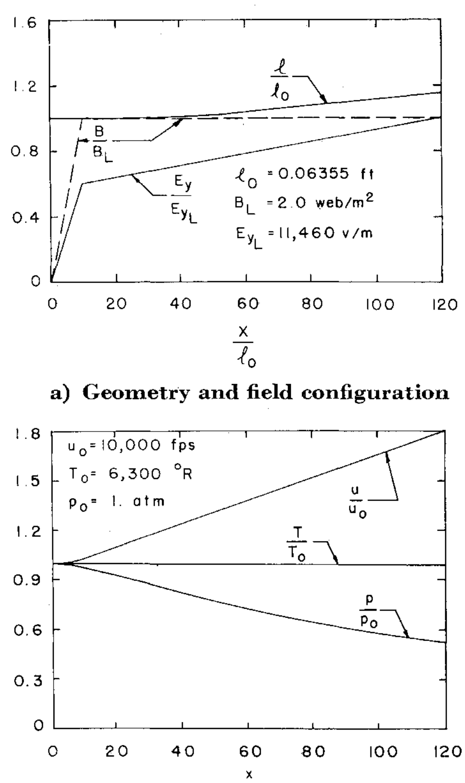

a) Geometry and field configuration

b) Core flow properties

Fig. 2 Streamwise variation of channel flow parameters using physically realistic recombination rate and energy-loss factor.

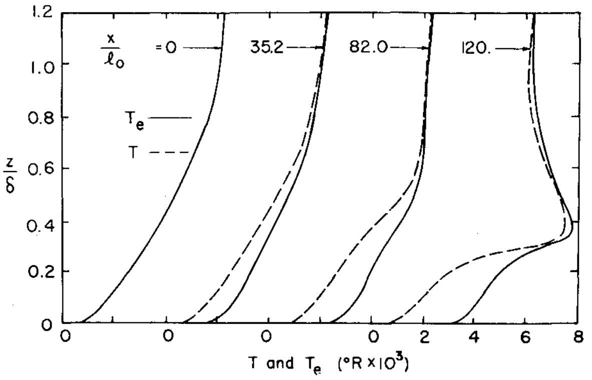

a) Over-all and electron gas temperatures

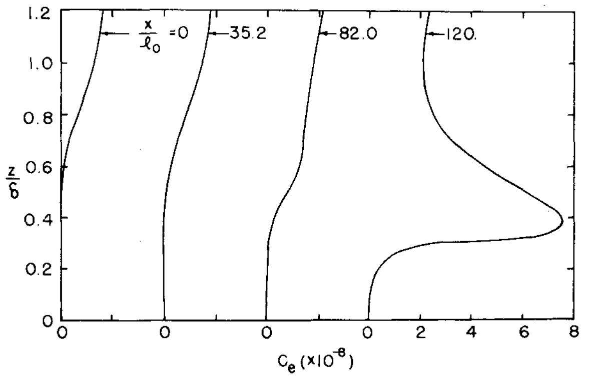

b) Electron concentration

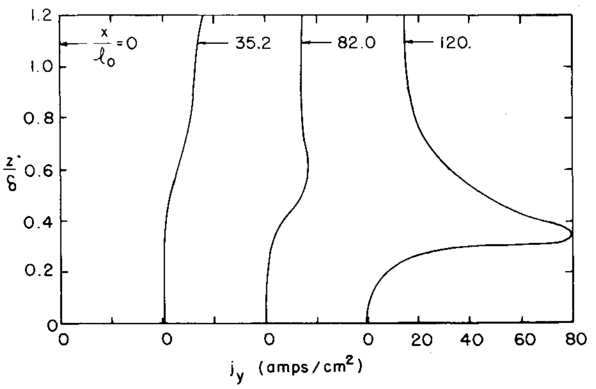

c) Transverse current density

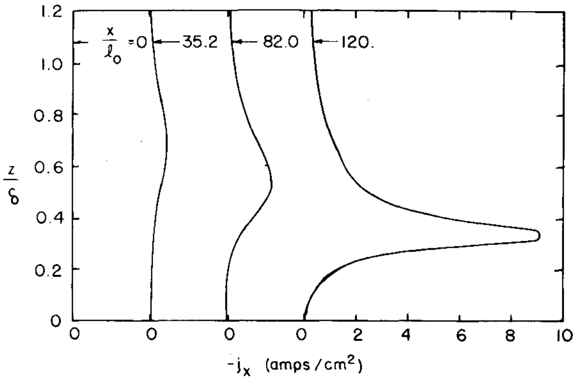

d) Hall current density

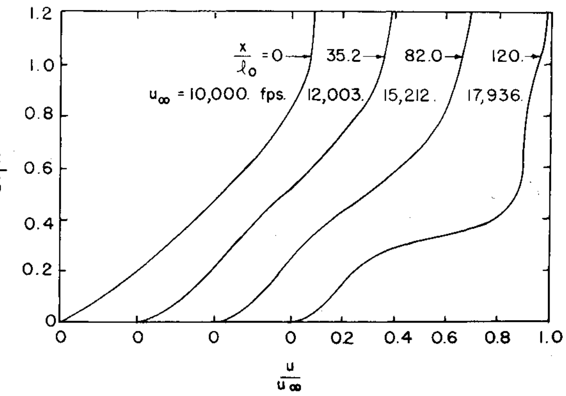

e) Velocity

Fig. 3 Development of boundary-layer profiles using physically realistic recombination rate and energy-loss factor.

3a and 3b, also display local maxima near the point of maximum current density. Thus Fig. 3 provides a picture of how B-wall shorting tends to amplify very quickly once it starts; with j increasing T_e and C_e through joule heating, which in turn leads to higher σ and hence increased j. The influence of the shorting of transverse current may be seen in Fig. 3e, which shows the resulting velocity hump at the accelerator exit.

Although it is not evident from Figs. 2 and 3, the dominant terms in the electron energy equation for this case are the joule heating terms and the collision term, with the conduction and diffusion terms becoming important only in the region where $z/\delta \leq 0.05$. One of the reasons why conduction and diffusion are of little importance is that the electrostatic sheath tends to insulate the electron gas from the cold, fully catalytic-wall. To illustrate this, at $x/l_0 = 120$ the wall temperature is 530°R, while the electron temperature at the outer edge of the sheath, $T_{e,0}$, is 1940°R.

Electron Thermal Nonequilibrium

To isolate the effects of electron thermal nonequilibrium the computer program was run for the same case as before, except with different values of energy-loss factor. The most physically realistic energy-loss factor is $\delta_{N_2} = 18$, according to Ref. 14. The lowest value of δ_{N2} which is reported in the literature is $\delta_{N_2} = 10$ (p. 148 of Ref. 4). This lower energy-loss factor leads to much higher electron temperatures, and so a case was computed with this value. For the equilibrium extreme, δ_{N_2} was simply multiplied by a factor of 10^4, to yield $\delta_{N_2} = 1.8 \times 10^5$.

Figure 4 compares the boundary layer profiles for $\delta_{N_2} = 10$, 18, and 1.8×10^5, at $x/l_0 = 82$. Smaller values of δ_{N_2} tend to severely aggravate the B-wall shorting problem, while no shorting at all exists for the case of electron thermal equilibrium ($\delta_{N_2} = 1.8 \times 10^5$). Keep in mind that these three cases were all run with the same recombination rate coefficient, given by Eq. (16).

Figure 5 shows the effect on local heat flux of varying the energy-loss factor. The plots of $\delta_{N_2} = 10$ are terminated beyond $x/l_0 = 85$, because severe B-wall shorting caused the electron temperature to exceed the range of validity of some of the assumptions used in evaluating the transport properties.

Ionizational Nonequilibrium

Several solutions were also computed with an energy-loss factor of 18 and different values of recombination rate coefficient, varying from frozen recombination to equilibrium recombination. The upshot of this phase of the investigation is that for the particular channel flow under consideration, the electron concentration is near equilibrium through the hotter portion of the boundary layer where shorting occurs. Considerable ionizational nonequilibrium exists near the cold wall, but here the electrical conductivity is so low that little current flows, and thus ionizational nonequilibrium has little effect on the over-all boundary layer.

Conclusions

For the class of nitrogen accelerators under study here, nonequilibrium effects are of secondary importance in laminar boundary layers to an x/l_0 of about ninety, but beyond that

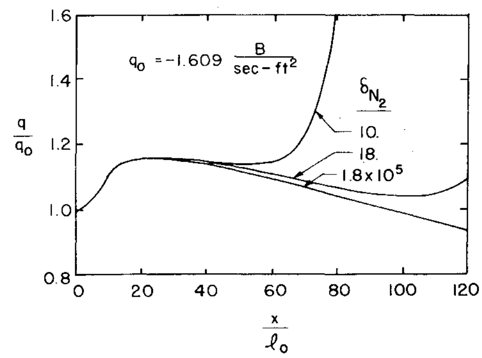

Fig. 5 Streamwise variation of local heat transfer for different values of energy-loss factor.

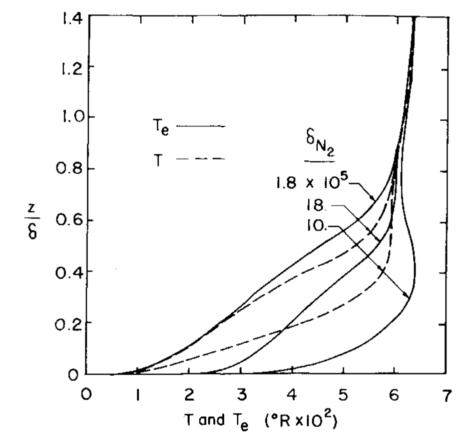

a) Electron and over-all gas temperatures

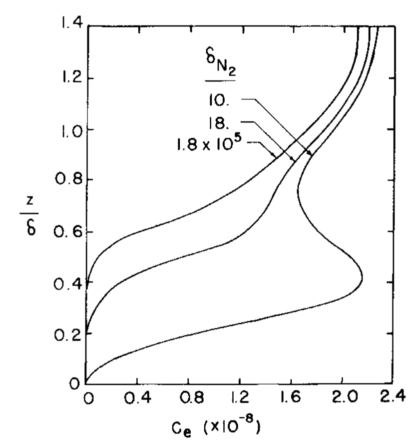

b) Electron concentration

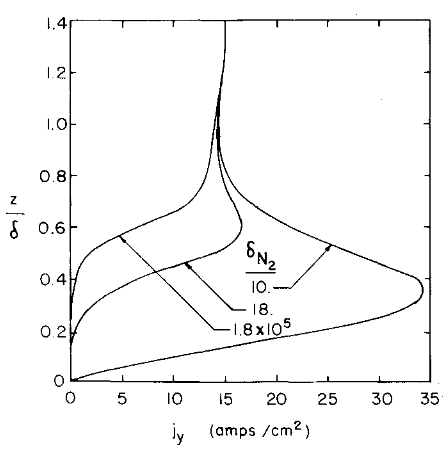

c) Transverse current

Fig. 4 Comparison of boundary-layer profiles at x/l_0 = 82.0, for different values of energy-loss factor.

point they are a direct cause of B-wall shorting. Once shorting begins, electron thermal nonequilibrium causes it to amplify very quickly, causing significant increases in heat transfer. If the channel is designed for equilibrium boundary layers, then the B-wall shorting is sufficient to cause thermal choking near the exit. Although there is considerable ionizational nonequilibrium in the colder portions of the boundary layer, it is insufficient in the hotter areas (where appreciable current flows) to affect the solutions noticeably. The relatively simple model of Hale and Kerrebrock,[1] which used only the collision and joule heating terms in the electron energy equation, and which assumed Saha equilibrium at the electron temperature, would have been quite adequate to describe the nonequilibrium effects for this application. While ionizational nonequilibrium is unimportant for the application studied here, it would be highly unwise to neglect it in other situations without careful consideration.

This study also points out the need for improved understanding of the basic collision phenomena involved in plasmas of engineering interest. For example, Figs. 4 and 5 demonstrate that the boundary-layer behavior is very sensitive to the value of the energy-loss factor. While reliable energy-loss data is abundant for low-temperature nitrogen and relatively high-energy electrons, it is very scarce for higher temperature gases involving lesser degrees of thermal nonequilibrium. Thus it should be emphasized that these boundary-layer calculations are only as good as the cross sections and energy-loss factors involved, and any future work undertaken should be based on improved evaluations of these quantities as they become available.

References

[1] Hale, F. J. and Kerrebrock, J. L., "Insulator Boundary Layers in MHD Channels," *AIAA Journal*, Vol. 2, No. 3, March 1964, pp. 461–469.

[2] Sherman, A., Yeh, H., Reshotko, E., and McAssey, E., "MHD Boundary Layers with Non-Equilibrium Ionization and Finite Rates," AIAA Paper 71-139, New York, 1971.

[3] Cott, D. W., "Ionizational and Electron Thermal Nonequilibrium Effects in Compressible MHD Boundary Layers," Ph.D. thesis, Dec. 1969, Univ. of Tennessee, Knoxville, Tenn.; also TR 70-231, Nov. 1970, Arnold Engineering Development Center, Arnold Air Force Station, Tenn.

[4] Sutton, G. W. and Sherman, A., *Engineering Magnetohydrodynamics*, McGraw-Hill, New York, 1965, Chaps. 4 and 5.

[5] Ring, L. E., private communication, Oct. 1968, Arnold Engineering Development Center, Arnold Air Force Station, Tenn.

[6] Baulknight, C. W., "The Calculation of Transport Properties at Elevated Temperatures," *Proceedings of the Second Biennial Gas Dynamics Symposium*, Northwestern University Press, Evanston, Ill., 1958, pp. 89–95.

[7] Curry, B. P., "Ionization and Recombination in Alkali-Seeded Collision-Dominated Plasmas," TR 65-260, Feb. 1966, Arnold Engineering Development Center, Arnold Air Force Station, Tenn.

[8] Cool, T. A. and Zukoski, E. E., "Recombination Rates and Nonequilibrium Electrical Conductivity in Seeded Plasmas," *The Physics of Fluids*, Vol. 9, No. 4, April 1966, pp. 780–796.

[9] Dugan, J. V., Jr., "Three-Body Collisional Recombination of Cesium Seed Ions and Electrons in High-Density Plasmas with Argon Carrier Gas," TND-2004, Oct. 1964, NASA.

[10] Demetriades, S. T., Argyropoulos, G. S., Lackner, K., and Kendig, A. P., private communication, Aug. 1967, STD Research Corporation, Pasadena, Calif.

[11] Weber, R. E. and Tempelmeyer, K. E., "Calculation of the D-C Electrical Conductivity of Equilibrium Nitrogen and Argon Plasma with and without Alkali Metal Seed," TDR-64-119, July 1964, Arnold Engineering Development Center, Arnold Air Force Station, Tenn.

[12] Demetriades, S. T. and Argyropoulos, G. S., "Ohms' Law in Multicomponent Nonisothermal Plasmas with Temperature and Pressure Gradients," *The Physics of Fluids*, Vol. 9, No. 11, Nov. 1966, pp. 2136–2149.

[13] Garrison, G. W., "Electrical Conductivity of a Seeded Nitrogen Plasma," *AIAA Journal*, Vol. 6, No. 7, July 1968, pp. 1264–1270.

[14] Demetriades, S. T., "Determination of Energy-Loss Factors for Slow Electrons in Hot Gases," *Physical Review*, Vol. 158, No. 2, June 10, 1967, pp. 215–217.

[15] Patankar, S. V. and Spalding, D. B., "A Finite-Difference Procedure for Solving the Equations of the Two-Dimensional Boundary Layer," *International Journal of Heat and Mass Transfer*, Vol. 10, No. 8, Aug. 1967, pp. 1389–1411.

[16] Patankar, S. V. and Spalding, D. B., *Heat and Mass Transfer in Boundary Layers*, Chemical Rubber Press, Cleveland, Ohio, 1968.